Available online at www.sciencedirect.com
ScienceDirect
Building and Environment 42 (2007) 1902–1912
BUILDING AND ENVIRONMENT
www.elsevier.com/locate/buildenv

Dispersion of gas pollutant in a fan-filter-unit (FFU) cleanroom

Sheng-Chieh Chen[a], Chuen-Jinn Tsai[a,*], Shou-Nan Li[b], Hui-Ya Shih[b]

[a]*Institute of Environmental Engineering, National Chiao Tung University, No. 75 Poai St., Hsin Chu, Taiwan, ROC*
[b]*Center for Environmental, Safety and Health Technology, Industrial Technology Research Institute (ITRI), Hsinchu, Taiwan, ROC*

Received 7 July 2005; received in revised form 18 October 2005; accepted 28 February 2006

Abstract

Numerical simulation and experimental measurement of flow and concentration fields in a working fan-filter-unit (FFU) cleanroom have been conducted in this study. The purpose of the study is to find out the unsteady concentration distribution of a leaking gas pollutant. The standard K–ε model was used for the simulation of the flow field. To obtain the gas concentration field, SF_6 gas with a certain concentration was released as a simulated leaking source from a valve manifold box (VMB) for 5 or 10 min, respectively. Three Fourier transform infrared spectrometers (FTIRs) were simultaneously used to measure the spatial and temporal distributions of SF_6 concentrations. The measured data were then compared with the numerical results and the agreement is seen to be quite good. From the numerical results, the pollutant hot spots, peak pollutant concentration at the end of leaking, and time taken for the concentration to reduce to near background level are obtained.

Keywords: Standard K–ε Model; Pollutant dispersion; Working cleanroom

1. Introduction

Numerous numerical and experimental studies on the flow field and pollutant dispersion in cleanrooms have been conducted. For example, Murakami et al. [1] found that turbulence is produced by physical obstructions in the cleanroom. Ljungqvist [2] pointed out that even at a low speed of 0.2 m/s, turbulence is still produced in the cleanroom and plays an important role in the diffusion of gases and particles. Thus, turbulence models should be applied to calculate the flow field of the cleanroom. Among various turbulent models, the standard K–ε two-equation model is the most widely used one, such as in [1,3–12]. Besides, Rouand and Havet [9] compared the Renormalization Group (RNG) K–ε model with the standard K–ε model and found that both models can predict the main features of the flow well. However, these researchers merely used simplified or pilot-scale cleanrooms to conduct their studies. Very few numerical studies investigate the airflow and pollutant dispersion in an actual working cleanroom, which has many existing process tools, partitions, ducts, exhaust gas abatement systems, workers, etc.

To further understand the gas dispersion patterns inside a working cleanroom, in this study, a SF_6 flow of 10,000 ppm was continuously released for 5 or 10 min around a valve manifold box (VMB) and its concentration variations were measured by three FTIRs. The on-site measurement data were then applied to compare with the numerical simulation results calculated by the standard K–ε model, which latter was used to estimate the spatial and temporal SF_6 concentration distributions inside the cleanroom and to locate the potential hot spots of high SF_6 concentrations.

2. Experimental method

The experiments were conducted in the furnace area (width 30 m × height 16 m × length 32 m) of a class 1, FFU type, semiconductor-manufacturing cleanroom, which is located in Hsin-Chu, Taiwan. Figs. 1(a) and (b) show the 2-D and 3-D schematic diagrams of the three-floor cleanroom, respectively, where the positions of the inlets, outlets, FFUs, and SF_6 leaking points are indicated. The

*Corresponding author. Tel.: +886 3 5731880; fax: +886 3 5727835.
E-mail address: cjtsai@mail.nctu.edu.tw (C.-J. Tsai).

0360-1323/$ - see front matter © 2006 Elsevier Ltd. All rights reserved.
doi:10.1016/j.buildenv.2006.02.023

Nomenclature

C	Courant number
C_μ, $C_{\varepsilon 1}$, $C_{\varepsilon 2}$	turbulence constants
F_s	diffusion flux component
k	turbulent kinetic energy (m^2/s^2)
l	turbulent mixing length (m)
ℓ	characteristic dimension (m)
m_s	mass fraction of the species (%)
p	static pressure (N/m^2)
u	fluid velocity (m/s)
V_n	superficial velocity normal to the surface of porous media
$\lvert\vec{V}\rvert$	a characteristic velocity (m/s)
x, y, z	Cartesian coordinates (m)
α, β	empirical coefficient
ΔP	airflow resistances (N/m^2)
Δt	iteration time step (s)
ε	turbulence energy dissipation rate (m^2/s^3)
μ	dynamic viscosity ($N\,s/m^2$)
μ_t	turbulent dynamic viscosity ($N\,s/m^2$)
μ_{eff}	$\mu+\mu_t$ ($N\,s/m^2$)
ρ	density (kg/m^3)
σ_k, σ_ε	turbulence constants
τ_{ij}	stress tensor components (N/m^2)

Subscripts

i, j, k	index of Cartesian components
s	species
c	1, 2, 3 for x, y, z directions, respectively

first floor is the sub-Fab area, the second is the Fab area, and the third is the supply air plenum. The airflow is moved by the FFUs, which are located at the ceiling of the Fab. For the working zones, 100% of the area is covered by the FFUs; for the machine maintenance zones, only 60% is covered by the FFUs.

Fig. 2 shows the floor plan of the Fab area in the cleanroom, which includes working zones, maintenance zones, machines, partitions, two SF_6 leak points, and doors. The top of the figure is adjacent to the central corridor while the bottom is adjacent to the recirculation duct. There are 695 FFUs on the ceiling of the Fab. For convenience, these FFUs were grouped into 16 square regions in our study. The FFUs in the working zones have smaller flow rate than that in the maintenance zones. The gas velocity at 0.3 m below the FFUs was measured by

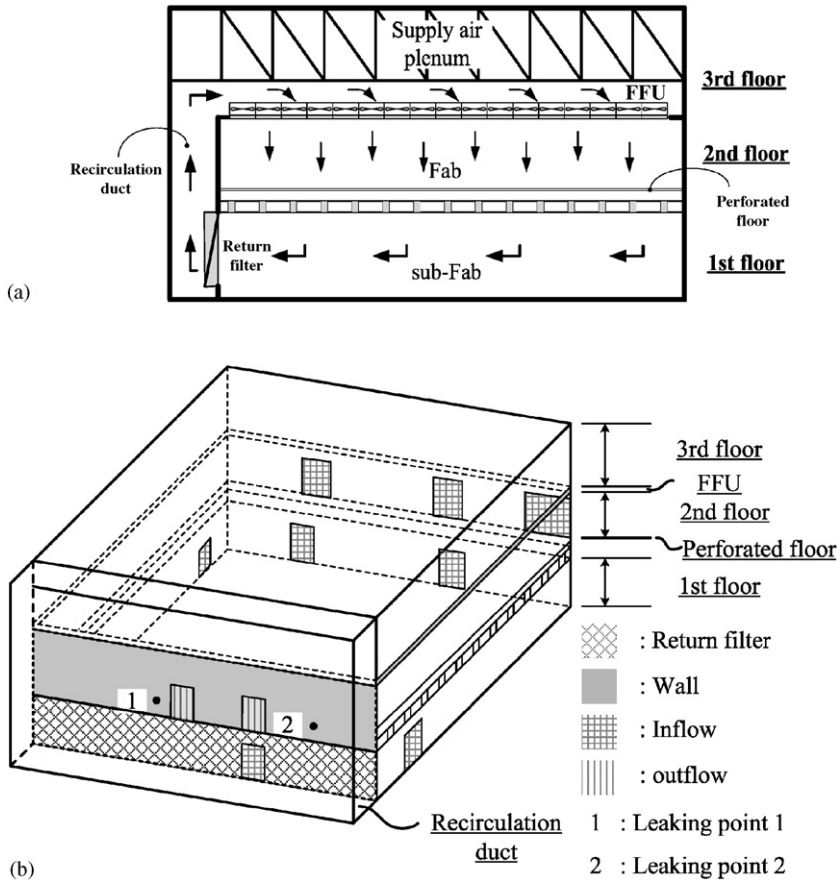

Fig. 1. (a) 2-D schematic diagram and airflow pattern in the FFU type cleanroom (width 30 m × height 16 m) (length is 32 m); (b) 3-D schematic diagram of the positions of the inlets, outlets, 16 FFUs, and the SF_6 emission points.

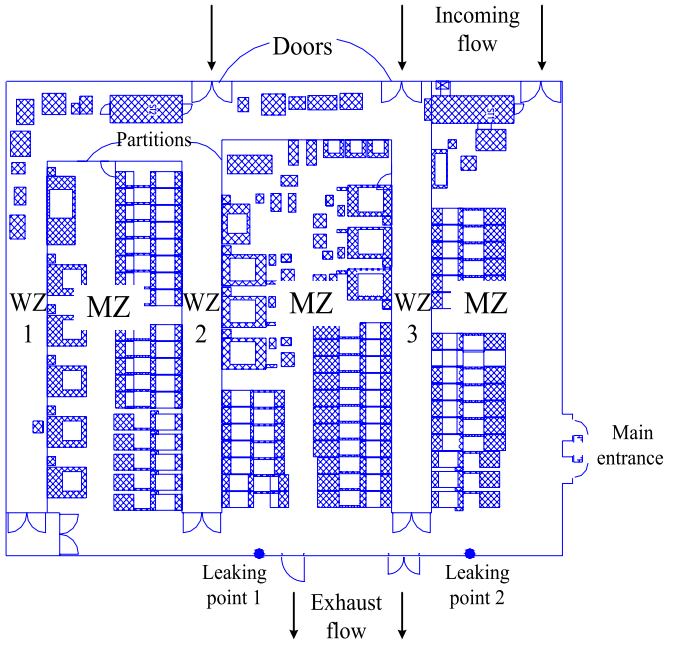

Fig. 2. The floor plan of the cleanroom, Fab area at the second floor. WZ: working zone, MZ: maintenance zone, and (⊠): Machines (top of the figure: adjacent to the central corridor, bottom of the figure: adjacent to the recirculation duct).

Table 1
Two different SF_6 releasing locations, concentrations and durations

	Flow rate (L/min)	Concentration (ppm)	Releasing (leaking) time (min)
Leaking point 1	10	10,000	10
Leaking point 2	10	10,000	5

using a TSI Model 8330 anemometer (TSI, Inc., St. Paul, MN, USA). The flow within 0.6–1 m below the FFU is unidirectional and perpendicular to the FFU when there is no obstruction underneath [12]. In this study, gas velocities were measured at 0.3 m below 10 different FFUs in each of the 16 regions. The averages of the 10 values were used to calculate the flow rate of each region by multiplying the area of the region and the percentage of area covered of the FFUs. The flow rates were used as the source momentums in the numerical simulation.

In a typical cleanroom flow, the make-up air is needed to maintain the air freshness in the cleanroom. For the cleanroom used in this study, the make-up air comes from the doors in the Fab (second floor) and the sub-Fab (first floor) areas. The original make-up air located in the sub-Fab does not function as initially planned because of air flow imbalance at different zones of the plant. On the other hand, the used air flow is exhausted directly through some doors and via two exhaust ducts connecting the equipments in the Fab and sub-Fab. The air flow rate through the exhaust ducts and doors were measured by the techniques similar to those used in the FFUs. For example, the area of each door was divided into nine equal parts for measuring the gas velocities at the center of these nine parts. The flow

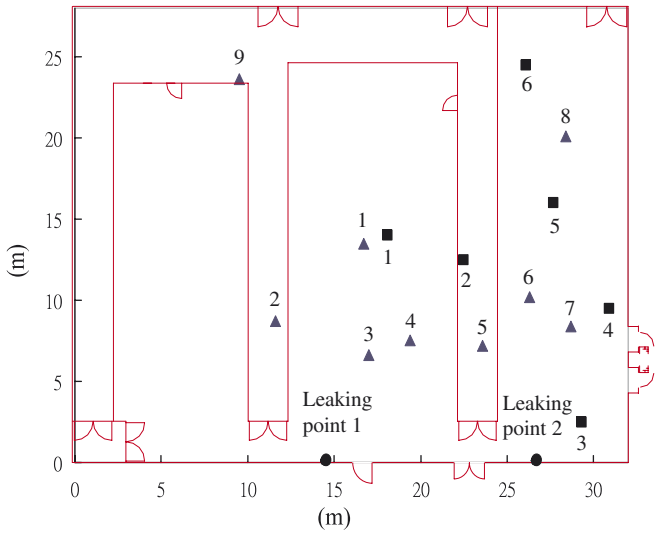

Fig. 3. Monitoring locations of SF_6 in the cleanroom: (△) leaking point 1, and (□) leaking point 2.

rate through each door was then determined. According to the experimental data, the recirculation and make-up air flow rates are about 900,000 and 85,000 CMH (m^3/h), respectively.

Two SF_6 leaking locations adjacent to the VMBs in the Fab are shown in Fig 2. A SF_6 flow of 10,000 ppm at 10 L/min was released horizontally into the Fab from point 1 or point 2 via a 1/4″ Teflon tube for 10 or 5 min, as summarized in Table 1. Three FTIR spectrometers (Model Work IR-104, ABB Bomem Inc., Quebec, Canada) with a detection limit of 10 ppb were located at three monitoring locations (10 cm above the perforated floor) to continuously measure the SF_6 concentrations for 50 min. SF_6 concentration is recorded every 5 s by the FTIRs. As shown in Fig. 3, for leaking point 1, nine locations (indicated as triangle symbols) were tested to obtain the SF_6 concentration variations; for leaking point 2, six locations (indicated as square symbols) were tested. To cover all monitoring locations, the three FTIRs were moved to three different locations to repeat the same experiment. The experiment was repeated three times for each monitoring location.

3. Numerical method

Steady state, incompressible flow is assumed in this study. The governing equations are the continuity and the Reynolds-averaged Navier–Stokes equations expressed as follows [13]:

$$\frac{\partial}{\partial x_j}(\rho u_j) = 0, \tag{1}$$

$$\frac{\partial}{\partial x_j}(\rho u_j u_i - \tau_{ij}) = -\frac{\partial p}{\partial x_i}, \tag{2}$$

where x is the coordinate (m), subscripts i and j are the index of Cartesian components, u is the fluid velocity (m/s),

ρ is the mass density (kg/m^3), τ_{ij} is the stress tensor (N/m^2), and p is the static pressure (N/m^2).

In order to obtain the turbulent flow field of the cleanroom, the standard K–ε model was employed in which the following two equations were solved:

$$u_j \frac{\partial k}{\partial x_j} = \frac{1}{\rho}\frac{\partial}{\partial x_j}\left[\frac{\mu_{\text{eff}}}{\sigma_k}\frac{\partial k}{\partial x_j}\right] + \frac{\mu_t}{\rho}\left(\frac{\partial u_i}{\partial x_j}+\frac{\partial u_j}{\partial x_i}\right)\left(\frac{\partial u_i}{\partial x_j}\right) - \varepsilon, \quad (3)$$

$$u_j \frac{\partial \varepsilon}{\partial x_j} = \frac{1}{\rho}\frac{\partial}{\partial x_j}\left[\frac{\mu_{\text{eff}}}{\sigma_\varepsilon}\frac{\partial \varepsilon}{\partial x_j}\right] + C_{\varepsilon 1}\frac{\varepsilon}{k}\frac{\mu_t}{\rho}\left(\frac{\partial u_i}{\partial x_j}+\frac{\partial u_j}{\partial x_i}\right)\left(\frac{\partial u_i}{\partial x_j}\right) - C_{\varepsilon 2}\frac{\varepsilon^2}{k}, \quad (4)$$

where μ_t is the turbulent viscosity (N s/m^2) defined as $\mu_t = C_\mu \rho k^2/\varepsilon$, and $\mu_{\text{eff}} = \mu + \mu_t$. The standard values of the model constants C_μ, $C_{\varepsilon 1}$, $C_{\varepsilon 2}$, σ_k, and σ_ε are $C_\mu = 0.09$, $C_{\varepsilon 1} = 1.44$, $C_{\varepsilon 2} = 1.92$, $\sigma_k = 1.0$, and $\sigma_\varepsilon = 1.22$.

The above equations were solved using the STAR-CD 3.15 code (CD-adapco Japan Co., Ltd.) which is based on the finite volume discretization method. The pressure–velocity linkage was solved by the semi-implicit method for pressure linked equation (SIMPLE) algorithm [14] and the differencing scheme for the space discretization method is the upwind differencing (UD) scheme. After the flow field was obtained, the unsteady state SF_6 concentration field was calculated based on the following mass conservation equation:

$$\frac{\partial}{\partial t}(\rho m_s) + \frac{\partial}{\partial x_j}(\rho u_j m_s - F_{s,j}) = 0, \quad (5)$$

where subscript s is the species, m_s is the mass fraction of the species, F_s is the diffusion flux component.

Multi-block, hexahedral cells were generated by an automatic mesh generation tool, Pro-Modeler 2003 (CD-adapco Japan Co., Ltd.). Various equipments in the cleanroom were simplified as rectangular blocks of the same size. The total number of cells used is about 1,200,000. The average cell length is around 0.25 m and the smallest length is 0.003 m (near the SF_6 leaking point). The cell size was enlarged gradually from the leaking point to avoid large jump between the sizes of two connected cells.

The convergence criterion of the flow-field calculation was set to be 0.3% for the summation of the residuals. Total number of iterations and the time required to reach convergence is about 500 and 200 min, respectively. The time step size, Δt, for transient calculation of the concentration field is determined by the Courant number C, which is a dimensionless quantity calculated as

$$C = \frac{|\vec{V}|\Delta t}{\ell}, \quad (6)$$

where $|\vec{V}|$ and ℓ are the characteristic velocity and dimension, respectively. In this study, we fixed C at 66.7 so that it was less than 100 as required by the cell-wise limited criteria [15]. Time step was determined to be 0.02 s. For leaking points 1 and 2, 30,000 (or 10 min) and 15,000 iterations (or 5 min) were required for simulating SF_6 leakage, respectively. Other 60,000 (20 min) iterations were required to calculate SF_6 decay for both leaking points.

3.1. Boundary conditions

No-slip condition was applied on the walls so that the velocities are zero at the boundaries except inlets and outlets. In addition, the wall function is implemented near the walls in order to avoid using too many grids near the walls. Uniform velocity distributions were assumed at the inlet and outlet boundaries based on the measurements. At the inlet boundaries, k and ε were given as $k = 1.5 \times (UI)^2$ and $\varepsilon = C_\mu^{0.75} \times k^{1.5}/l$, where U is the inlet velocity (m/s), I is the turbulent intensity, and l is the turbulence length scale (m). The criterion for selecting l is suggested to be one order of magnitude less than the length of the boundary (STAR-CD User Guide, 2003). In this study, l was set to be 0.1. According to the measurements, the exhaust flow rates through the machines tools were set to be 60% and 40% at the outlet boundaries of the Fab and sub-Fab, respectively. The gradient of k and ε at the outlet boundaries is zero.

In the pollutant dispersion calculation, SF_6 was set as a scalar boundary and l was set to be 0.005. The releasing SF_6 flow rates and its concentrations are shown in Table 1.

The flows of FFUs were modeled as momentum sources based on the measured data. In order to simplify the simulation, the FFUs were divided into 16 individual regions as mentioned previously. In each region, the source momentum term was defined by a subroutine so that the simulated flow rate matched the experimental data.

Three parts of the cells in the cleanroom were defined as porous media to simulate the airflow resistance in this study. The first part is the perforated floor, the second is the filters of FFUs, and the last is the return filters. The airflow resistances ΔP in these units can be expressed as [16]

$$\Delta P = \alpha_c V_n^2 + \beta_c V_n, \quad (7)$$

where subscript $c = 1$, 2, 3 for x, y, z directions, respectively; α and β are parameters related to inertia and viscosity, respectively; V_n is the superficial velocity normal to the surface of porous media. According to the experiment and manufacturer's data, α and β can be calculated by Eq. (7) and the values are shown in Table 2.

Table 2
Parameters of porous media

	α_1	β_1	α_2	β_2	α_3	β_3
Perforated floor	1000	1000	1000	1000	50	50
FFU	1000	1000	1000	1000	30	30
Return wall filter	300	300	50	50	300	300

4. Results and discussions

The accuracy of the flow field calculation significantly affects the SF_6 concentration distribution. Therefore it is necessary to validate if the flow field is accurate. In the simulated results, it is found that the flow is restricted in the vertical, downward direction only (or z direction, V_z) with the maximum turbulence intensity $<2\%$ for about 0.5 m below the FFU. The simulated results of V_z are compared with the experimental data at 0.3 m below the FFU, as shown in Fig. 4. It can be seen that the agreement between the measured and simulated velocities is very well with the maximum difference of 4.8% only. The results also show that the working zones of the cleanroom have lower velocity of 0.27–0.33 m/s while the maintenance zones have higher velocity of 0.43–0.52 m/s.

After an accurate steady-state flow field was obtained, the unsteady-state SF_6 concentration distribution was then calculated. In the FTIR measurements of SF_6 concentration, the experiment was repeated at the same location for three times. Fig. 5 shows the temporal distributions of the three data sets for location 3 shown in Fig. 3. The maximum difference is only about 5 ppb. Similar precision can also be found in other monitoring points. That is, the FTIRs used in this study are reliable and the experimental data can be used to examine the accuracy of the simulated results.

4.1. SF_6 concentration distribution

The SF_6 concentration distributions at the perforated floor surface after leaking for 10 (leaking point 1) and 5 min (leaking point 2) are shown in Figs. 6 and 7, respectively. In Fig. 6, it can be seen that the SF_6 concentration over half of the cleanroom is higher than 35 ppb, and the highest is about 50 ppb at the leaking time of 10 min (leaking point 1). With shorter leaking time of 5 min for leaking point 2, the highest concentration is also about 50 ppb. However, only 1/8 of the cleanroom has SF_6 concentration higher than 35 ppb. This indicates that longer leaking time results in a wider spread of accumulated gas in the cleanroom. A longer leaking time of 50 min was also simulated for leaking point 1 to see whether the maximum SF_6 concentration at the perforated floor kept on increasing with leaking time. Simulated results reveal that the maximum SF_6 concentration will increase to about 70 ppb after 20 min of leaking but this maximum value does not increase further after 20 min.

For the case of leaking point 1 shown in Fig. 6, the high concentration region on the perforated floor first appears in front of the leaking point. As leaking continues, the region gradually spreads into the center of the cleanroom until the end of leaking. For leaking point 2, the high concentration region shown in Fig. 7 looks much smaller than that of Fig. 6. This difference is due to the inference of the local flow distribution on the gas transport. The flow field near leaking points 1 and 2 is shown in Fig. 8, where it indicates the used cleanroom air flowing out through the two doors. The flow on the cleanroom floor (top figure of Fig. 8) is seen to converge toward these two doors. The influence of the local exhaust flow on the concentration field is stronger for leaking point 2 than for leaking point 1, which results in the shift of the high concentration region to the left of leaking point 2. The region is also much smaller due to "SF_6 sink" at these two exhaust doors.

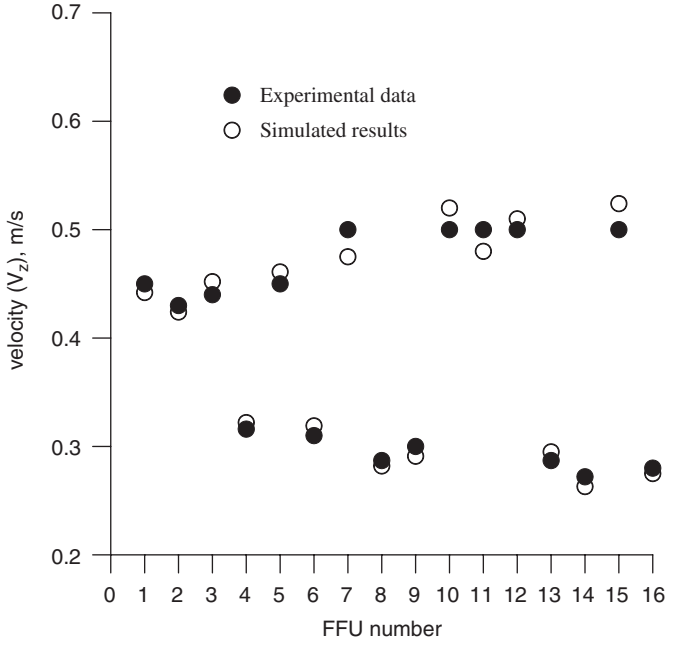

Fig. 4. Comparison of experimental gas velocities with simulated results at different FFU locations.

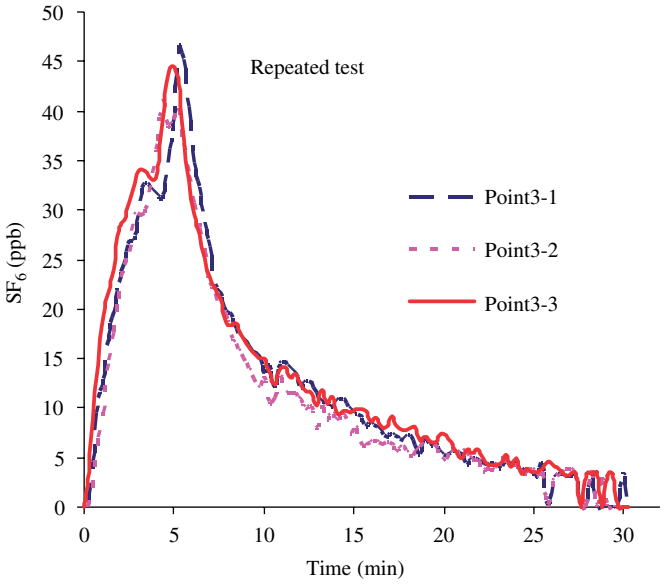

Fig. 5. Repeated SF_6 measurements at the same location using the FTIR spectrometer.

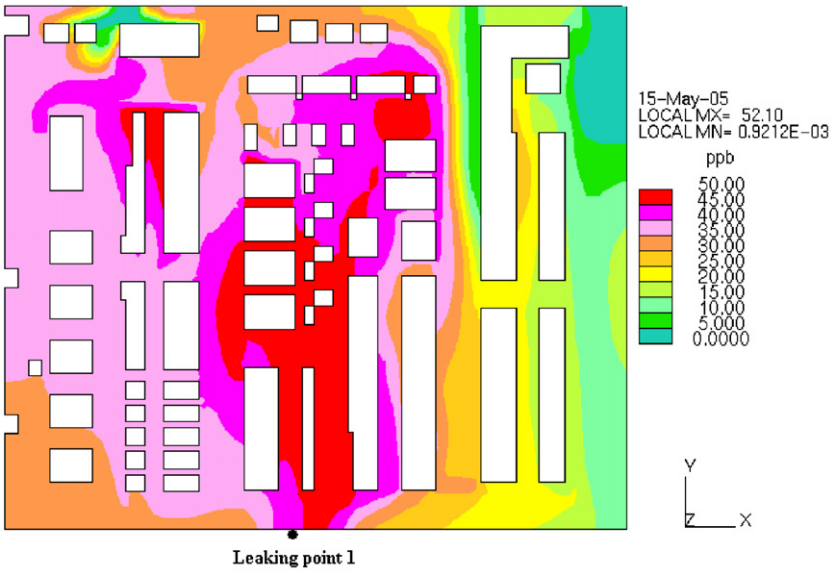

Fig. 6. Simulated SF_6 concentration profile on the perforated floor at the end of 10 min leak, leaking point 1. White region: tools.

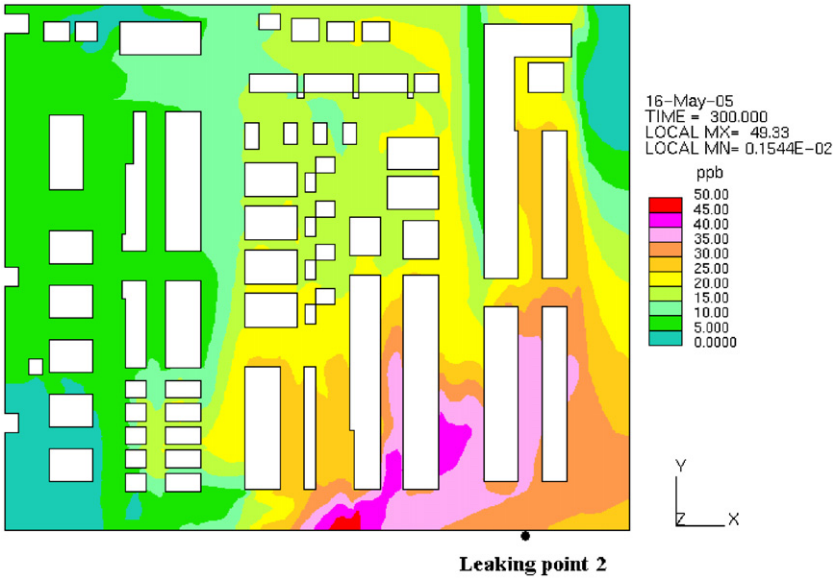

Fig. 7. Simulated SF_6 concentration profile on the perforated floor at the end of 5 min leak, leaking point 2.

Comparatively lower SF_6 concentration regions can be found near the top of Figs. 6 and 7, where it is farther away from the leaking points, and the incoming flow through the three doors has a strong dilution effect. Near the top rightmost corner of the cleanroom, the SF_6 concentration appears to be the lowest because of a strong clean air entering this region with a flow rate of 7.3 m^3/s through the door. Therefore, to obtain better gas dispersion results inside a cleanroom, it is important to know the gas leakage location and the incoming and exiting flow directions. A complete understanding of the gas concentration distribution is very crucial to better protect the workers' health and enhance the product (wafer) quality [17,18].

4.2. Comparison of experimental and Numerical SF_6 concentrations

Figs. 9 and 10 show the comparison of SF_6 concentrations between the numerical results and experimental data for leaking point 1 (nine measured points) and leaking point 2 (six measured points), respectively. The SF_6 concentration is seen to increase with leaking time until leaking stops in both figures. After leaking stops, the SF_6 concentration decays with time but at a slower rate. Small differences of less than 30% between the experimental data and numerical results are observed when SF_6 concentrations are higher than 10 ppb. The differences become larger

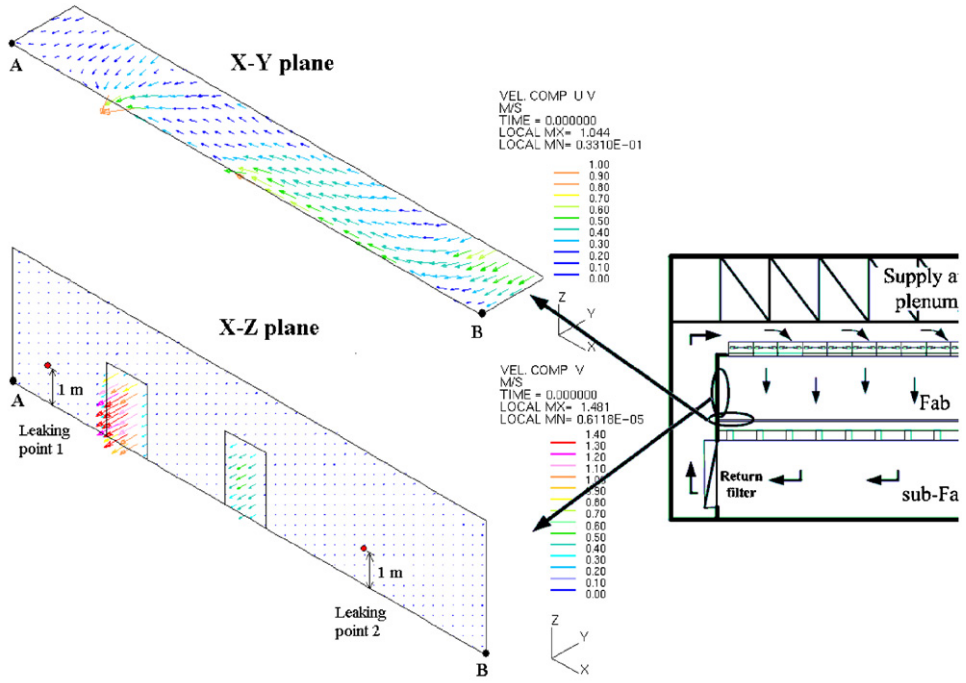

Fig. 8. Simulated flow field near the two leaking points. Upper figure: the flow field in the cleanroom at the perforated floor, horizontal plane; lower figure: flow field in the cleanroom near the leaking points, vertical plane (next to the recirculation duct).

when the SF_6 concentrations are lower than the detection limit of the FTIRs, 10 ppb.

In general, the comparison is quite well for leaking point 1 when the monitoring points, such as points 1–4, are near the leakage. If the monitoring points are farther from the leaking point, such as points 5–9, the concentration is lower and the agreement decreases. Point 7 has the maximum difference since it is close to the Fab entrance and measurement was affected by the workers, beside its lower SF_6 concentration. Similar results are found for leaking point 2, although the SF_6 concentration is in general lower than that of leaking point 1.

When the leaking stops, the SF_6 concentration decays with time. For the concentration to drop below 10 and 5 ppb, the time required is about 13 and 19 min, respectively, for leaking point 1 (total leaking time is 10 min). For leaking point 2 (total leaking time is 5 min), the time taken for SF_6 concentration to drop below 10 and 5 ppb is about 5 and 10 min, respectively. That is, the longer the leakage is, the longer it takes to recover the cleanroom to a "clean" condition.

4.3. Hot spots of SF_6

As described earlier, the peak SF_6 concentration on the cleanroom floor increases with leaking time with a maximum of only 50 ppb, except near the leaking point. After careful examination of the SF_6 concentration field in the entire cleanroom, an exceptionally high concentration region is found in the recirculation duct. After leaking for as short as 10 s (leaking point 1) or 20 s (leaking point 2) only, a region with SF_6 concentration higher than 100 ppb is found, as shown in Figs. 11(a) and (b), respectively. For leaking point 1, the maximum concentration in the recirculation duct is found to increase very rapidly in the first 10 s to 470 ppb, and the value remains almost the same (about 500 ppb) until the end of leaking (10 min), as shown in Fig. 12. This value is about 10 times the maximum concentration on the cleanroom floor, which is 50 ppb after 10 min of leaking. For leaking point 2 (Fig. 11(b)), the maximum SF_6 concentration in the recirculation duct is about 200 ppb after 20 s of leakage and this maximum concentration also remains nearly the same until leaking stops (5 min), as shown in Fig. 12. That is, high SF_6 concentration region appears in the recirculation duct at an elevation near the bottom of the perforated floor, as soon as gas leakage occurs. The maximum concentration in the duct is nearly 10 or four times the peak SF_6 concentration in the cleanroom, for leaking point 1 or 2, respectively.

In order to find out the reason why there is a high SF_6 concentration region in the recirculation duct, the flow field near the duct is shown in Fig. 13. It is found that there is a dead recirculation zone close to the wall just behind the leaking point at a level near the perforated floor. The SF_6 concentration is accumulated very rapidly to a high concentration which persists in the recirculation region until leakage stops.

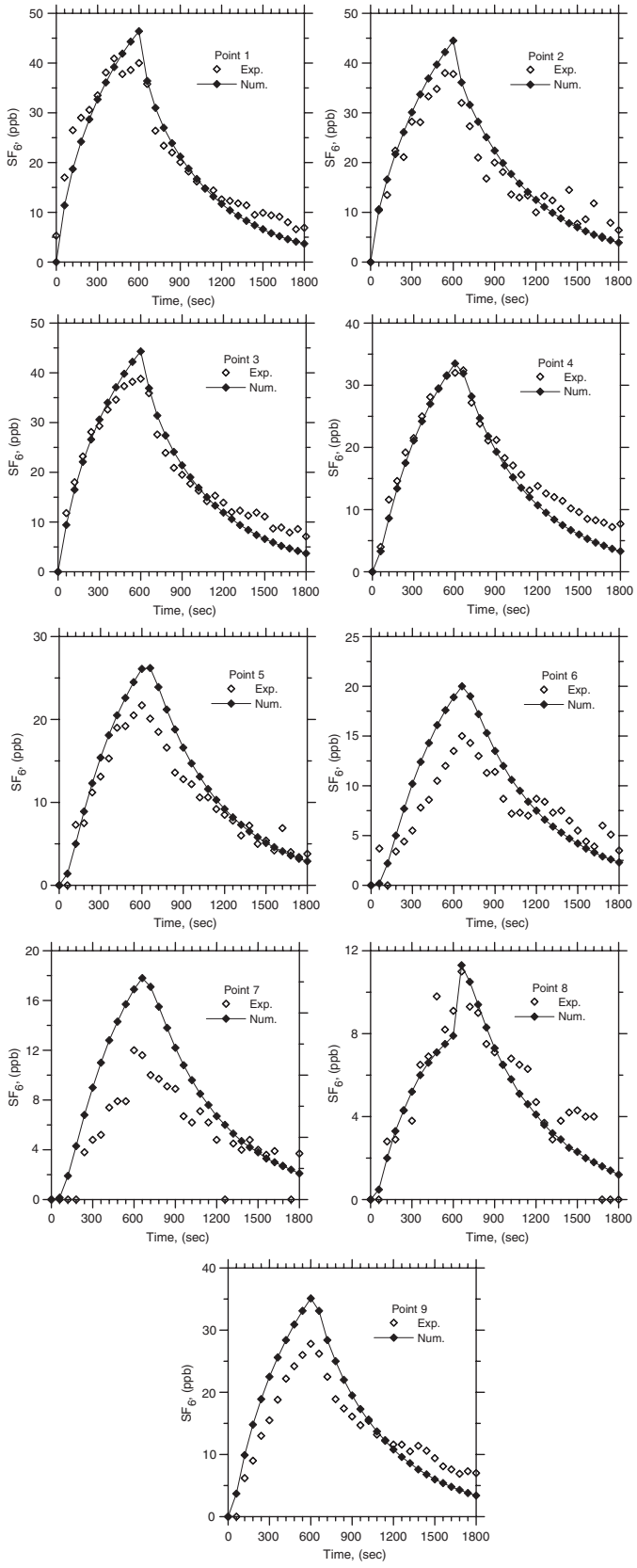

Fig. 9. Comparison of experimental SF_6 concentrations with simulated results at different measurement locations, leaking point 1.

In summary, the hot spot is found in the recirculation duct at an elevation near the bottom of the perforated floor, where the gas concentration increases very rapidly to a high value with an increasing leaking time.

We further simulated the concentration field assuming leaking of SF_6 occurs at the center of the cleanroom and in the downward direction. The released time, SF_6 concentration, and the leaking flow rate are 10 min, 10000 ppm, and 10 slmp, respectively. High SF_6 concentration region is also found inside the recirculation duct at the elevation near the bottom of the perforated floor. After leaking for 30 s, the SF_6 concentration is about 200 ppb and a high concentration region exists near the center of the duct.

4.4. *Effect of make-up air flow rate and leaking SF_6 concentration on SF_6 dispersion*

Further simulations were conducted to study the effect of make-up air flow rate and leaking SF_6 concentration (fixed leaking flow rate at 10 slpm) on SF_6 dispersion in the cleanroom, especially in the recirculation duct and at the perforated floor. The leakage was fixed at leaking point 1. The results are shown in Table 3, where the peak SF_6 concentrations at the recirculation duct and the perforated floor are found to increase almost linearly with the leaking SF_6 concentration when the make-up air flow rate is fixed at 85,000 CMH. As the SF_6 concentration is increased from 5000 to 10,000 and 50,000 ppm, the peak SF_6 concentration at the perforated floor is increased from 25 to 50 and 250 ppb, respectively; the peak SF_6 concentration in the recirculation duct is increased from 250 to 500 and 2600 ppb, respectively. This is to be expected since the flow field does not change if only the SF_6 leaking concentration changes. Increasing the make-up air flow rate from 85,000 to 255,000 CMH also leads to a nearly linear decrease of peak SF_6 concentration at both recirculation duct and the perforated floor. The peak SF_6 concentrations in recirculation duct and the perforated floor are reduced from 500 to 160, and from 50 to 15 ppb, respectively. However, the SF_6 concentration does not increase, rather it decreases when the make-up air flow rate is reduced from 85,000 to 42,500 CMH. This is because when the flow field is changed, the dispersion of SF_6 is also changed. Table 3 also shows the effect of leaking SF_6 concentration and make-up air flow rate on the time taken for the SF_6 concentration to decrease to the background level (5 ppb). As the make-up air flow rate increases from 42,500, 85,000 to 255,000 ppm, the time taken to reduce to background level is reduced almost linearly from 36, 19 to 6.5 min, respectively. On the other hand, by increasing the SF_6 concentration from 5000, 10,000 to 50,000 ppm, the time taken for SF_6 to reduce to background level does not increase linearly. It increases from 11, 19 to 36 min, respectively.

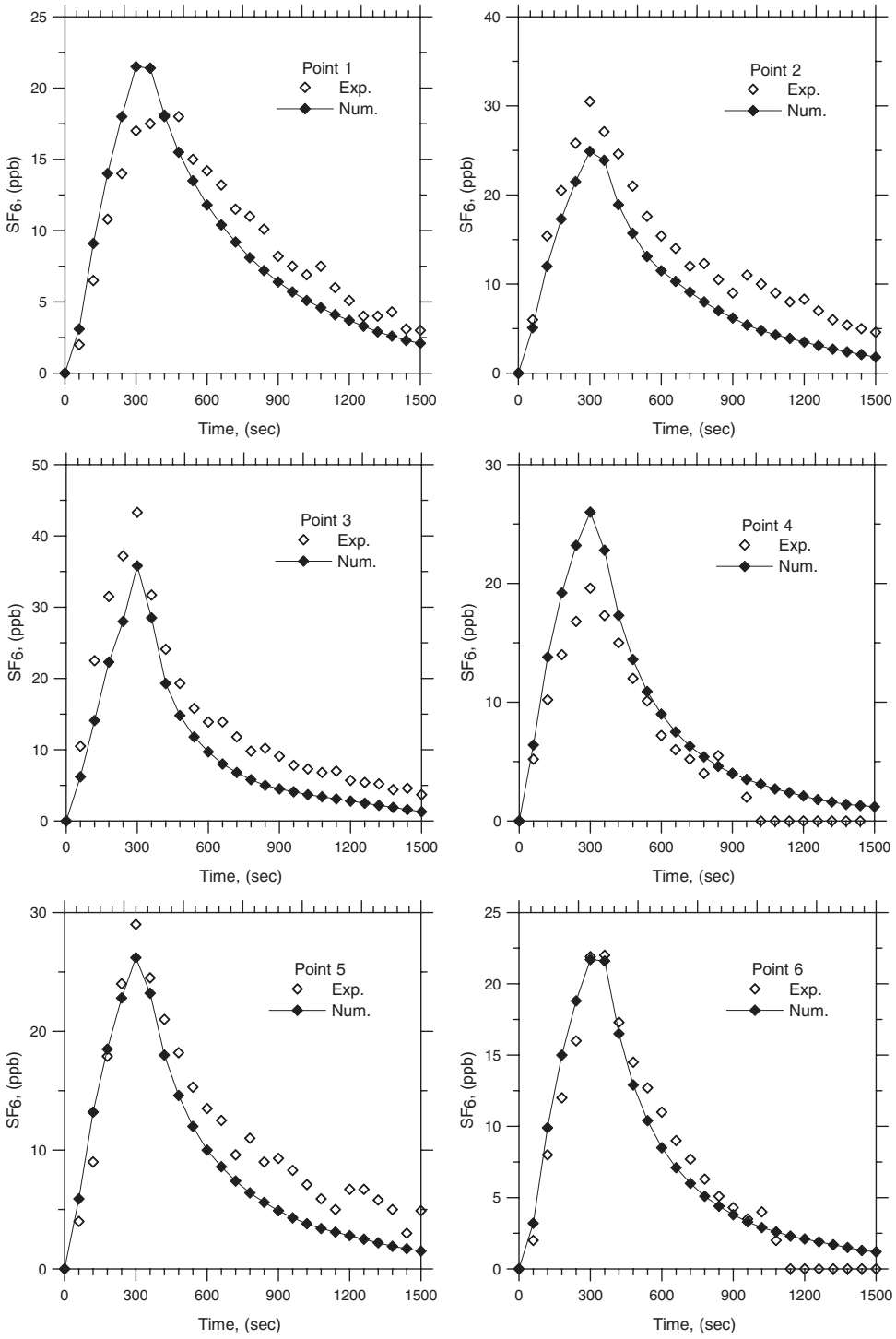

Fig. 10. Comparison of experimental SF_6 concentrations with simulated results at different measurement locations, leaking point 2.

5. Conclusion

Experimental and 3-D numerical studies were conducted in a working FFU type cleanroom of a semiconductor manufacturing plant to find the unsteady-state pollutant distribution in the cleanroom. SF_6 gas was used as a tracer gas to simulate gas leakage near the VMBs in the Fab. FTIR spectrometers were used to measure the SF_6 concentration field and the collected data were then used to compare with the simulation results. The simulation model is found to predict the mean flow velocities and the SF_6 concentration fields very well. Small differences of less than 30% between the experimental data and numerical results are observed when the SF_6 concentrations are higher than 10 ppb.

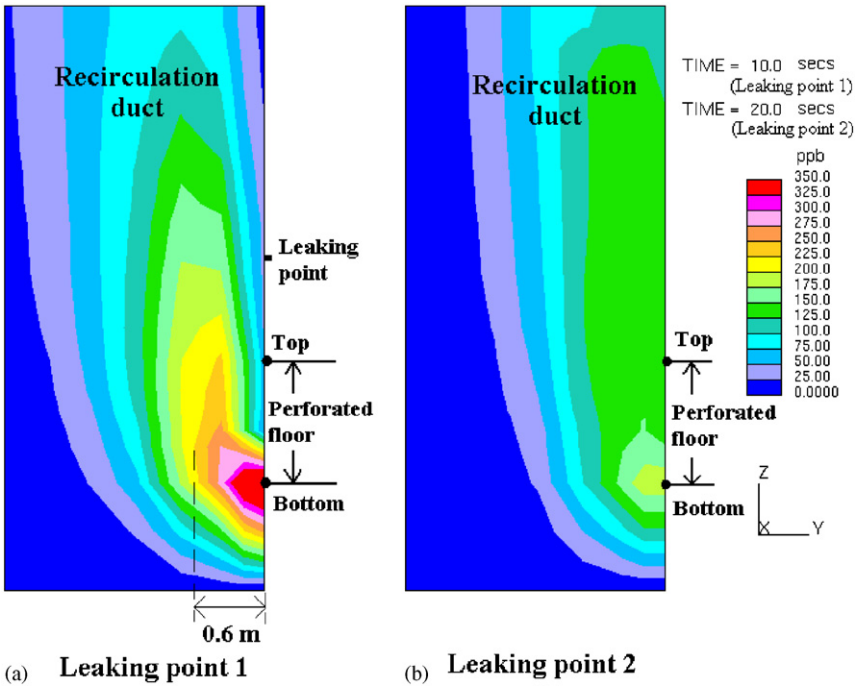

Fig. 11. Simulated SF_6 concentration in the recirculation duct after leaking for: (a) 10 s, leaking point 1 and (b) 20 s, leaking point 2.

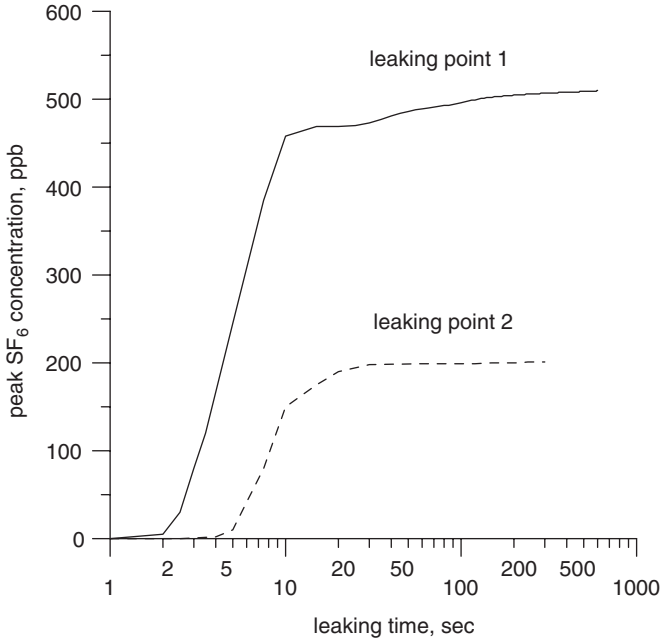

Fig. 12. Maximum SF_6 concentration in the recirculation duct during gas leakage.

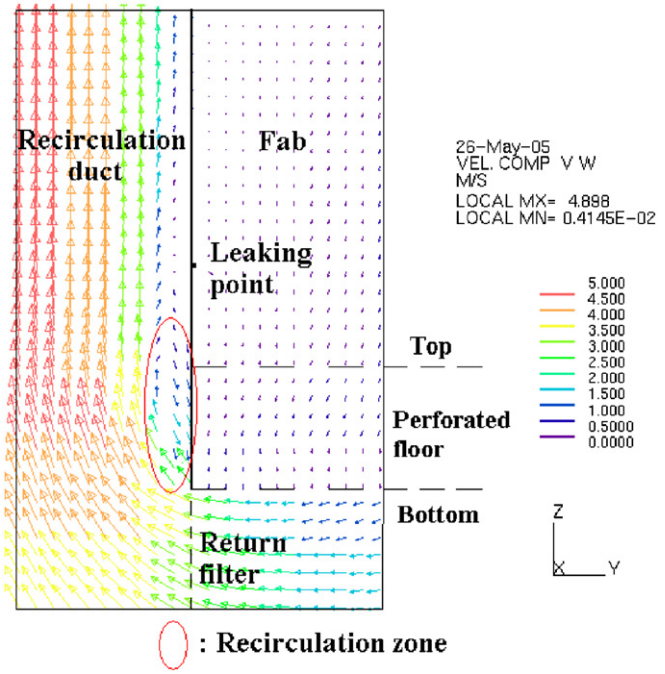

Fig. 13. Velocity field in the recirculation duct (width: 2.5 m, height: 11 m, length: 32 m).

The SF_6 concentration field in the cleanroom is found to depend on the leaking position, local inflow or outflow disturbance and the field varies with leaking time. The maximum concentration in the cleanroom increases with an increasing leaking time and is not high because of the dilution power of the make-up air. We found a dead recirculation zone close to the wall at a level near the perforated floor where the SF_6 concentration accumulates very rapidly and persists until the end of leaking. The peak gas concentration in the recirculation duct is about 10 times the peak concentration found in the cleanroom.

Table 3
Effect of make-up air flow rate and leaking SF_6 concentration on SF_6 dispersion[a]

Leaking point 1, 10 min leaking	SF_6: 10,000 ppm Make-up air: 85,000 CMH	SF_6: 10,000 ppm Make-up air: 255,000 CMH	SF_6: 10,000 ppm Make-up air: 42,500 CMH	SF_6: 50,000 ppm Make-up air: 85,000 CMH	SF_6: 5000 ppm Make-up air: 85,000 CMH
Peak SF_6 conc. at perforated floor (ppb)	50	15	48	250	25
Time to reduce to background level, 5 ppb (at perforated floor) (min)	19	6.5	36	36	11
Peak SF_6 conc. in the recirculation duct (after leaking for 20 s) (ppb)	500	160	490	2600	250

[a]SF_6 leaking flow rate is fixed at 10 slpm.

Acknowledgement

Authors would like to thank for the financial support of this project by the Industrial Technology Research Institute (ITRI) in Taiwan in 2004.

References

[1] Murakami S, Kato S, Suyama Y. Numerical study of flow and contaminant diffusion fields as affected by flow obstacles in conventional-flow-type cleanroom. ASHRAE Transactions 1990;96(Part 2):343–55.
[2] Ljungqvist B, Reinmuller B. Clean room design/minimizing contamination through proper design. Buffalo Grove: Interpharm Press; 1997. p. 3.
[3] Murakami S, Kato S, Suyama Y. Three-dimensional numerical simulation of turbulent airflow in a ventilated room by means of a two-equation model. ASHRAE Transactions 1987;93(Part 2):621–42.
[4] Murakami S, Kato S, Suyama Y. Numerical and experimental study on turbulent diffusion fields in conventional flow type cleanrooms. ASHRAE Transactions 1988;94(Part 2):469–93.
[5] Murakami S, Kato S, Suyama Y. Numerical and experimental study on diffusion field as affected by arrangement of supply and exhaust openings in conventional flow type cleanrooms. ASHRAE Transactions 1989;95(Part 2):113–27.
[6] Kato S, Murakami S. New ventilation efficiency scales based on spatial distribution of contaminant concentration aided by numerical simulation. ASHRAE Transactions 1988;94(Part 2):309–30.
[7] Nam S. Numerical simulation of smoke movement in cleanroom environments. Fire Safety Journal 2000;34:169–89.
[8] Cheng M, Liu GR, Lam KY, Cai WJ, Lee EL. Approaches for improving airflow uniformity in unidirectional flow cleanrooms. Building and Environment 1999;34:275–84.
[9] Rouaud O, Havet M. Computation of the airflow in a pilot scale cleanroom using K–ε turbulence models. International Journal of Refrigeration 2002;25:351–61.
[10] Hu SC, Chuah YK, Huang SC. Performance comparison of axial fan fan-filter unit (FFU) type cleanrooms by CFD. ASHRAE Transactions 2002;AC-02-17-4:1014–22.
[11] Hu SC, Chuah YK. Deterministic simulation and assessment of air-recirculation performance of unidirectional-flow cleanrooms that incorporate age of air concept. Building and Environment 2003;38:563–70.
[12] Kozicki M, Hoenig S, Robinson P. Cleanrooms facilities and practices. New York: Van Nostrand Reinhold; 1991.
[13] Computational Fluid Dynamics Software. STAR-CD Version 3.15. Methodology. London: Computation Dynamic Limited; 2000.
[14] Patankar SV. Numerical heat transfer and fluid flow. Washington: Hemisphere Publishing Co; 1980.
[15] Computational Fluid Dynamics Software. STAR-CD version 3.15. User guide. London: Computation Dynamic Limited; 2000.
[16] Nield DA, Bejan A. Convection in porous media. New York: Springer; 1992.
[17] Li SN, Chang CT, Shih HY, Li A, Chen YY. Using an extractive fourier transform infrared spectrometer for improving cleanroom air quality in a semiconductor manufacturing plant. AIHA Journal 2003;64:408–14.
[18] Li SN, Shih HY, Wang KS, Hsieh K, Chen YY, Chou J. Preventive maintenance measures for contamination control. Solid-State Technology 2005;53:56.